Estimating wind erosion threshold based on dust optical depth data in Northern Africa.

Author: ELISA BERGAS MASSÓ
Supervisors: MARTINA KLOSE[1], martina.klose@bsc.es; CARLOS PÉREZ[1], carlos.perez@bsc.es; YOLANDA SOLA[2], ysola@ub.edu; MIREIA UDINA[2], mudina@ub.edu*
[1]*Earth Sciences Department, Barcelona Supercomputing Center (BSC), Barcelona, Spain.*
[2]*Facultat de Física, Universitat de Barcelona, Diagonal 645, 08028 Barcelona, Spain.*

Abstract: Dust emission is initiated when surface wind velocities exceed a threshold of wind erosion that depends on soil and surface conditions. Dust emission models incorporate poorly constrained wind erosion threshold values as there is a lack of the required data, especially in regions known as dust emission sources. Here, we consider the possibility of using high-resolution satellite data to retrieve wind erosion thresholds. The main difficulty of using satellite observations for this purpose is the quantification of the separate contribution of transported dust and emited dust at a single location from the total dust column mass load observed at that place. However, biases due to that underlying problem have not been assessed because there is no direct observation quantifying only emissions. In this study, the potential biases over Northern Africa are investigated using simulated dust emission flux and optical depth from the Multiscale Online Non-hydrostatic Atmospheric Chemistry (MONARCH) model developed at the Barcelona Supercomputing Center. Assuming that the model fully reproduces the connection between these two variables, we show that the threshold is underestimated by more than 50% in regions where there is only transported dust. On the other hand, over dust emission sources, the absolute relative error is smaller. An alternative method based on the fact that the emission flux is considered to be proportional to the cube of the friction velocity is explored. A further refinement of these methods can help improve the simulations of dust climatology and seasonal cycle as well as dust forecasting.

I. INTRODUCTION

Airborne mineral dust, emitted predominantly from soils in arid and semi-arid regions, is an important atmospheric constituent and represents by mass about 40% of the global annual emissions of tropospheric aerosols (*Solomon et al.* 2007). Dust can directly affect human beings and their everyday life by causing respiratory diseases and infections (*Cook et al.* 2005) or reducing visibility with severe consequences on air traffic, road transportation, and military operations (*Pauley et al.* 1996). Atmospheric mineral dust has a key role within the Earth system by contributing to a variety of physical, chemical, and biogeochemical processes. For instance, transported and deposited dust over oceans acts as a source of micronutrients and it is also thought to be an essential fertilizer for the Amazon forest (*Prospero et al.* 2014). Mineral particles absorb and scatter short and longwave radiation, consequently modifying the local energy budget and circulation patterns (*Woodward* 2001). In addition, dust particles play a role in cloud microphysics by serving as ice nuclei (*Min et al.* 2009) and when deposited on snow and ice, the surface albedo is altered (*Wittmann et al.* 2017).

Given the significance of airborne dust for weather and climate, understanding the processes of the dust cycle represents a key challenge when developing atmospheric and climate models. The first step to fully reproduce the dust cycle is to build a reliable dust emission scheme.

Dust is emitted from dry and uncovered soil surfaces. As soon the wind exceeds a threshold value, wind erosion is initiated and dust particles are emitted through bombardment by saltating sand grains. This wind erosion threshold is the result of the balance between the forces that hold soil particles at the surface (weight and interparticle cohesion forces) and those that drive particle lifting (aerodynamic drag and lifting forces) (*Shao and Lu* 2000). The threshold thus depends on soil and surface conditions, such as soil moisture, surface roughness elements or particle size, which change in space and time.

The wind erosion threshold is thus one of the fundamental variables in dust emission schemes. However, a method to retrieve the global distribution of the wind threshold and its variability is still needed especially because of a lack of in-situ data on soil surface properties in regions considered as dust sources. Consequently, dust models use varying degrees of simplification to estimate the wind erosion threshold.

There has been an attempt in estimating the wind erosion threshold using satellite observations in *Pu et al.* (2019). Detection of mineral dust from satellite observations relies on variables that depend on specific optical properties of dust particles. The vertically integrated coefficient of extinction, by aborption and scattering, of solar radiation by airborne dust particles at a given wavelength is referred to as dust optical depth (DOD). DOD is used as an indicator of the dust load of particles in an atmospheric column. It is important to point out that DOD is then not only accounting for dust being emitted at a single place but also airborne dust that has been

* Electronic address: ebergama7@alumnes.ub.edu

advected from other regions.

In this study, we aim to investigate the possibility of using DOD retrived from satellite observations to infer the wind erossion threshold. As dust emission cannot be observed directly from satellite, there is no means to validate the resulting threshold values when using DOD data. For this purpose, instead of using satellite observations, model data corresponding to one-year simulation using MONARCH, the Multiscale Online Nonhydrostatic AtmospheRic CHemistry model (*Pérez et al.* 2011), is used for which both dust emission fluxes, DOD and other meteorological variables, and surface characteristics are given.

After analyzing to what extent the magnitude and variations of dust emission fluxes can explained through DOD data, we seek to find and evaluate a reliable method for retreiving the wind erossion threhold distribution from DOD data.

The following section describes the model configuration, resulting datasets and methodology used. Section III describes the results and their discussion and in Section IV, we draw the main conclusions and examine future prospects.

II. DATA AND METHODOLOGY

A. Data

In this study we use a one-year simulation obtained with the MONARCH (*Pérez et al.* 2011). The data used in this study are 3-hourly output of accumulated dust emission flux [kg/m^2], instantaneous DOD, and instantaneous friction velocity (u^*) [m/s]. The data set is gridded with 1° and 1.4° of latitudinal and longitudinal grid spacing respectively.

The largest areas with high frequency of dust emission are located in the Northern Hemisphere, mainly in the so called dust belt that extends from the west coast of North Africa, over the Middle East, Central and South Asia, to China (*Prospero et al.* 2002). In this work, we focus on North Africa, where the most important dust source areas in the world, in terms of dust mass load magnitude and frequency, are located: the Bodélé depression in Chad and an area in the southwestern Sahara Desert region of Mali, Mauritania, and Algeria (*Koven and Fung* 2008). In particular, the domain of this study has been selected following the same criterion of *Shao et al.* (2013), with the lower left corner at 30°W, 0°N and the upper right corner at 34°E, 40°N. The land surface of the domain considered can be appreciated in Fig.(3).

The atmospheric flow pattern in this region, and hence the dust emission, are mainly driven by seasonal contrasts regulated by the intertropical convergence zone (ITCZ). The ITCZ can be seen as a transition zone in the surface between the dry northeasterly harmattan air and the moist air from the equatorial regions. The ITCZ advances northward from February to June or August, when it attains its maximum latitude, then retreats southward until December (*Nicholson* 2018). Over West Africa the advection is in this manner generally linked to the northeasterly harmattan winds blowing from the Sahara across the semiarid Sahel toward the Guinea coast of Africa with the ITCZ limiting the southward penetration of the dust (*N'tchayi Mbourou et al.* 1997).

The following subsections summarize briefly the configuration of the model that has been used to obtain the dust emission flux and DOD data sets that are used in this study.

1. *Dust emissions modeled with MONARCH*

MONARCH includes serveral dust emission schemes. In the MONARCH model simulation used in this study, dust emission was estimated using the parameterization from *Marticorena and Bergametti* (1995) in which dust saltation bombardment is defined as the key process that generates airborne dust. The model simulates the horizontal saltation flux (H) for different particle size according to (*White* 1979):

$$H_i \propto \frac{\rho_a}{g} u_*^3 \Big(1 + \frac{u_{*t_i}}{u_*}\Big)\Big(1 - \frac{u_{*t_i}^2}{u_*^2}\Big) s_i \quad \text{for } u_* > u_{*t_i} \quad (1)$$

where ρ_a is the air density, u_* is the wind friction velocity which is predicted by a surface layer scheme which follows Monin-Obukhov similarity theory, g is the gravitational acceleration constant, u_{*t} is the threshold wind friction velocity and s_i is the relative surface area of each particle size class i at every grid cell.

The threshold wind friction velocity is estimated as

$$u_{*t} = u_{*tsd}(D_s)\frac{f_h}{f_e} \quad (2)$$

where $u^*_{tsd}(D_s)$ is the threshold friction velocity of a smooth and dry surface with soil particles of diameter D_s, which is parameterized with a semi-empirical relationship that takes into account the density of the soil particles and its diameter (*Iversen and White* 2006). The correction parameter f_h takes into consideration the fact that soil water can inhibit dust emission by increasing the threshold friction velocity of soil particles and ranges from 1 (for nearly dry surface) and increases with volumetric soil moisture (*Fécan et al.* 1999). Finally, f_e is the so-called drag partition correction parameter and expresses the efficiency with which drag is partitioned between the roughness elements characterized by an aerodynamic (or aeolian) roughness length (z_0) and the erodible surface characterized by a smooth roughness length (z_{0s}) (*Marticorena et al.* 1997). f_e ranges from a value close to 0, meaning very efficient partition to 1, meaning no-partition.

The model transforms horizontal to vertical dust emis-

sion flux following an empirical relationship (*Marticorena and Bergametti* 1995) by which the vertical dust flux (F) is proportional to the horizontal sand flux (H). The proportionality is estimated based on the soil's clay content, as this is considered to be the soil fraction responsible for dust particle abundance.

2. NMMB-MONARCH Dust Optical Thickness

The dust optical thickness τ is calculated from the dust mass load using the following equation:

$$\tau(\lambda) = \sum_i \frac{3}{4} \frac{Q_{ext}(\lambda, r_i) M_i}{r_i \rho_i} \tag{3}$$

where $Q_{ext}(\lambda, r_i)$ is the extinction efficiency at wavelength λ and effective radius r_i, and M_i and ρ_i are the column mass loading and mass density for the size class i respectively. MONARCH uses 8 size classes to represent the size distribution of dust.

It should be remarked that although in the model one can differentiate between the optical depth of dust and that of other aerosols, when using remote-sensing observations this is not as straightforward. Satellite data has to be typically filtered and the coarse-aerosol (particle size greater than 1 μm radius) is commonly associated with mineral dust. To be consitent in this study and be able to better compare modeled DOD with filtered observed DOD, the coarse mode DOD from the model will be used. The DOD data set used in this study has thus been computed for particles larger than 2 μm in diameter.

B. Methodology

All the algorithms for data and image processing developed in the present study have been created using the programming environment R-Cran (R-Cran Team, 2013).

With the purpose of establishing and evaluate a reliable method for retrieving the wind erosion threshold using DOD data, this study make use, as already mentioned, of NMMB-MONARCH model outputs for which both DOD and emission data are given.

The correlation between both variables is firtly analyzed to see if the relation is stronger in a particular season or time of the day.

Afterwards, two different methodologies are tested. The first one is based on the assumption that the frequency of occurrance (FoO) of DOD exceeding a threshold can be used as a proxy for identifying dust source areas (*Ginoux et al.* 2012). The hypothesis is that the threshold will be exceeded more frequently at or close to dust source areas. The second method, relies on the thesis that a linear relation between the magnitude of DOD and emission can be established so an increase of the magnitud of the emission flux is reflected as an increase in DOD in a given proportion. A function of the form of Equation 1 can be under this hypothesis fitted to DOD data and in this way obtain the wind emision threshold values.

1. Relationship between DOD and Emission

With the aim of using satellite observations of DOD as a constraint to model emissions or infer the wind erossion threshold, one must first quantify the proportion of the variance in emissions that can be explained by DOD. A linear regression fit (Equation 4) to modeled DOD versus emissions data is established in order to quantify the coefficient of determination (R^2) between both variables. The resulting slope (a) represents the rate of DOD change per unit change in the emission flux and the intercept (b) represents the level of background DOD.

$$DOD = a \cdot F + b \tag{4}$$

The goodness and confidence of the fitted parameters will be sought by season and time of the day. Furthermore, an exoploration of the possibility of a time lag between emission and DOD data will be carried out, meaning that the instantaneous DOD could be higher correlated with emissions from the the previous time step outputed by the model.

2. Method to Estimate the Wind Erosion Threshold

Once the seasons or months in which the relationship in Equation 4 gets maximized are identified, meaning that DOD data at a given time and location is dominated by emissions at the same location, the study proceeds to propose and evaluate two different methods to determine the wind erosion threshold.

(i) In the first method (FoO Method), the threshold of wind erosion is retrieved by matching the frequency distribution of the modeled DOD above a certain level with the frequency distribution of wind friction velocities over a given period in every grid cell. The process can be summarized by the following steps:

1) First step is to calculate, on a daily basis, the FoO when DOD exceeds a threshold value (in %), here we consider a threshold value of 0.2 as stated by *Ginoux et al.* (2012).

2) Next, the inverse cumulative frequency distribution of wind friction data at every grid cell is computed (% of cases in which the u_* exceeds or equals a certain value).

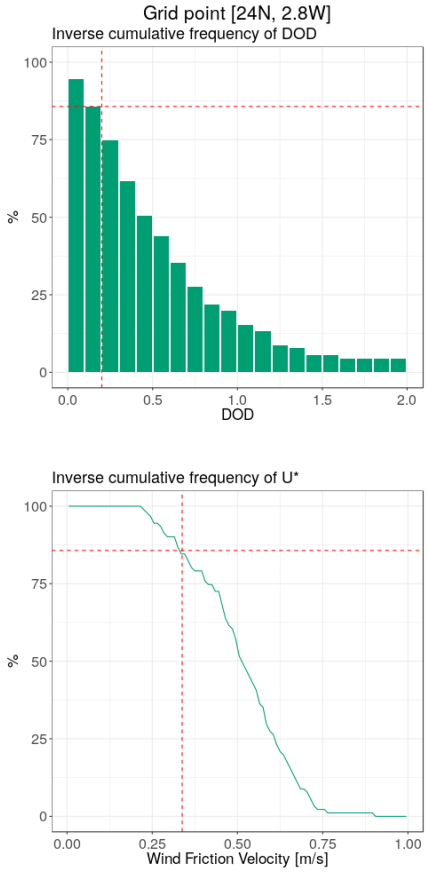

Figure 1. A scheme of the procedure to derive the wind erosion threshold at one location. The upper figure represents the frequency of DOD above incresing DOD values. The bottom figure shows the inverse cumulative frequencies of wind friction velocities at the same location. The red vertical line in the upper figure corresponds to a value of DOD of 0.2 and its corresponding frequency is indicated by the horizontal one. The frequency found above is then matched with the figure below to get the wind erosion threshold (vertical red line of the bottom figure).

3) The FoO of DOD that has been established in step 1 is then compared with the inverse cumulative frequencies of winds. The minimum wind friction with the same frequency corresponds to the threshold of wind erosion (see a schematic diagram in Figure 1).

(ii) A second different method to retrieve wind erosion threshold is proposed in this study. In this other method (Fitting Method) the main assumption is that the change in magnitude at a given time and location of DOD is proportional to the change of magnitude of emission flux. By assuming that, DOD data in function of wind friction velocities in every grid cell should also follow a function of the form of Equation 1. There are two unknown parameters when fitting DOD data to the equation, one of them the searched wind erosion threshold itself. The main motivation of testing this other method is that in this way, one can get more information of DOD values than when using only frequencies.

As previously mentioned, DOD data not only accounts for dust being emitted at one particular place but also dust that has been transported to there. With the purpose of fitting the given function to DOD data that might be more influenced by emissions than transport, the DOD is filtered by wind friction. This implies that the fit is only done using DOD data in which the corresponding wind friction is exceeding a certain value.

The algorithm for fitting and parameter estimation makes use of iteratively reweighted least squares (IRLS) with a non-linear least squares approach. A further insight to the theoretical explanation of this algorithm is out of the scope of this work.

Referring back to what has been already mentioned, the gains of doing this study with model output data is that an evaluation of the proposed methods can be carried out. The resulting wind threshold fields with both methods are compared to the ones used in the simulation by estimating the relative error (RE) at every grid cell (Equation 5).

$$RE_i = \frac{u_{*tr_i} - u_{*tm_i}}{u_{*tm_i}} \cdot 100 \tag{5}$$

where RE_i is the relative error at the grid cell i in percent and, u_{*tr_i} and u_{*tm_i} are the retrieved and used by the model wind erosion threshold respectively.

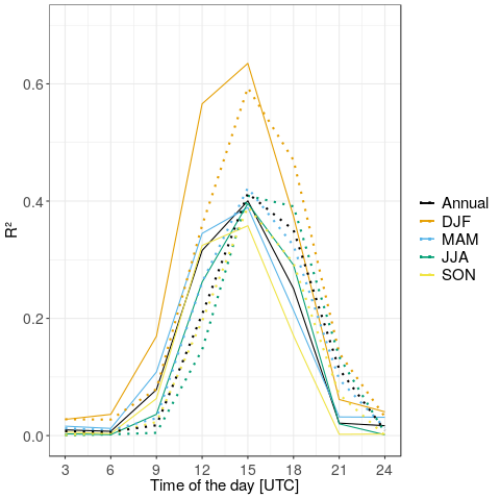

Figure 2. Correlation coefficient of the variables DOD and dust emission 3-hourly accumulation flux for every time of the day and season. Dashed lines correspond to the correlation between DOD at that time of the day with the emission flux of the previous time step.

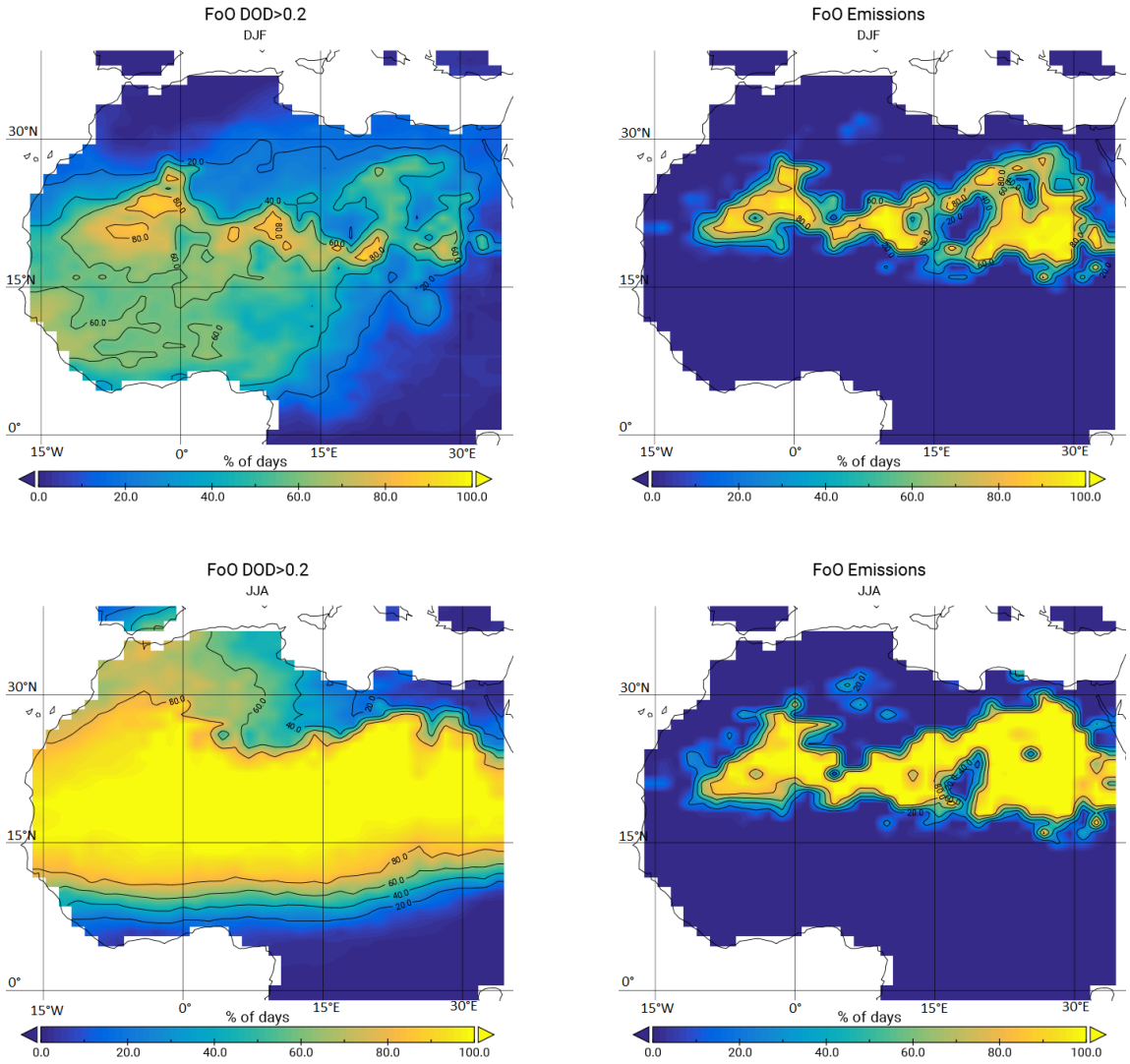

Figure 3. Frequency of occurrence (in % of days) of dust optical depth exceeding a value of 0.2 in North Africa for DJF (upper left corner) and JJA (lower left corner) seasons. At the right side, the corresponding frequencies of occurrence of emissions are presented.

III. RESULTS AND DISCUSSION

A. Relationship between DOD and Emission

As can be seen in Fig.(2), there is a significant dependency on the time of the day in the goodness of the correlation between DOD and emissions. During night time, the correlation coefficient clearly drops and it is maximum at mid-day hours (12-15 UTC). That could be given by the fact that dust emission events are considered to be promoted at peak heating hours when atmospheric instability increases and strong winds are prone to occur (*Knippertz* 2008). At low-emission hours, correlation between these two variables decreases as there may be still airborne dust remaining from intense emission-hours resulting in an instantaneous DOD value that is not well explained by emissions at the same output hour.

If a comparison between seasons is made, a significant increase in the correlation during the December-January-February (DJF) season can be detected. Winter corresponds to harmattan winds reaching lower latitudes than during any other season. However, emission events are inhibited in this season due to a more stable atmosphere (*Cowie et al.* 2014). Dust transport is in that way also reduced.

The possibility of a 3-hour time-lag between emission and DOD data is also considered and as Fig.(2) shows, this occurs mostly in the afternoon when DOD correlates better with emissions at noon as the amount of particle dust emitted at that time is larger and is still in suspension.

Although the maximum correlation is observed at 15

UTC the data analysis of the following sections are performed considering only 12 UTC data. We make this decision because 12 UTC resembles more the time of a polar satellite overpass over this region.

season	a (std.error) [m^2/kg]	b (std.error)	R^2	r
DJF	259.7 (0.5)	0.07279 (0.00018)	0.275	0.525
MAM	314.3 (0.8)	0.2893 (0.0005)	0.150	0.388
JJA	337.1 (1.0)	0.2617 (0.0005)	0.131	0.362
SON	324.2 (1.0)	0.10506 (0.00019)	0.118	0.343
Annual	320.7 (0.4)	0.18243 (0.00019)	0.145	0.380

Table I. Coefficients of the linear regression (a and b) and coefficients of determination (R2) and correlation (r) for every season taking into account all time steps.

season	a (std.error) [m^2/kg]	b (std.error)	R^2	r
DJF	208.0 (0.6)	0.0638 (0.0004)	0.564	0.751
MAM	265.8 (1.1)	0.2651 (0.0012)	0.346	0.588
JJA	272.7 (1.4)	0.2418 (0.0012)	0.264	0.514
SON	275.2 (1.2)	0.0976 (0.0005)	0.325	0.570
Annual	264.2 (0.6)	0.1668 (0.0005)	0.317	0.563

Table II. Coefficients of the linear regression (a and b) and coefficients of determination (R2) and correlation (r) for every season taking into account only 12 UTC ouput data.

As seen in Table I and II correlation coefficients are much lower if the correlation is determined with all time steps together and resulting slopes of Equation (4) are higher. This last fact helps to support the idea that at night the variables correlate worse as the dominant airborne dust at that moment is the one emitted at previous hours at the same place or advected from other locations. When establishing the correlation with all output time data, the resulting slope increases as for less emission the correspondent DOD is higher. Table II shows that the slope values (a) range from about 200 to 275 [m^3/kg] and the intercept (b) from around 0.05 to 0.3.

B. FoO Method

The FoO of DOD exceeding 0.2 has been computed for DJF and June-July-August (JJA) at 12 UTC to compare seasonal differences. The FoO of emissions is also determined to have a view of the correspondence between the FoO fields of both quantities (Fig.(3)). It can be noticed that the FoO of DOD using DJF data is a much better approximation to the FoO of emissions that for JJA, as the main dust emission sources can be better distinguished from locations where there is only transported dust.

However, if we attempt to use the FoO of DOD at DJF as if it was equivalent to the FoO of emissions, we then have underestimations over emission sources and overestimation over regions where dust is transported. It is apparent that during DJF months transport dominates from emission sources at around 20° to the southwest reaching the Gulf of Guinea. As mentioned previously, during DJF the ITCZ reaches the southernmost latitude and harmattan winds transport dust to these regions. As a result, FoO of DOD over these locations is overestimating the FoO of emissions.

Comparing the distribution of the FoO of emissions for both seasons, it iz shown than dust emission sources in JJA cover more area than that in DFJ and the frequency of events slightly increases over regions that show emissions during both seasons. This is something that we expected because as mentioned previously, during DJF emissions are inhibited.

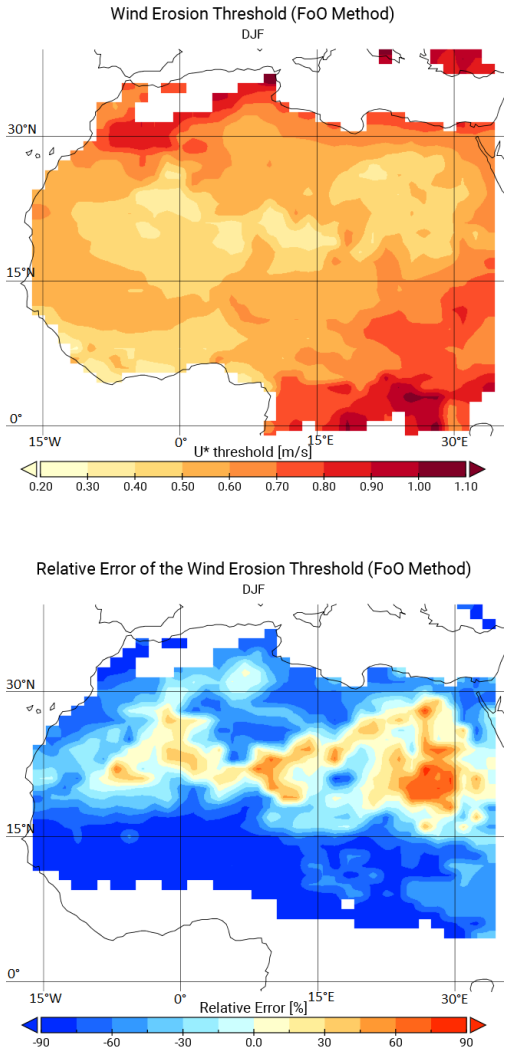

Figure 4. The upper figure presents the wind erosion threshold distribution retrieved through the FoO method using DJF data. In the bottom figure, the relative error between the model-used wind friction threshold velocity and the corresponding retrieved wind erosion threshold for DJF (reddish colors indicate overestimation and blue indicate underestimation).

After computing the FoO of DOD, the wind erosion threshold is retrieved with the FoO method. The wind erosion threshold distribution using DJF data (upper Fig.(4)) shows similar patterns to the FoO of DOD at that season, meaning that in places where the FoO of DOD over 0.2 is high, the retrieved wind erossion threshold is low and the other way around. That results in a wind erosion threshold around 0.3 m/s over the Sahara and northern side of the Gulf of Guinea while in other regions such as the Atlas or the southern sector of the region of study, the wind erosion threshold can reach values above 1 m/s.

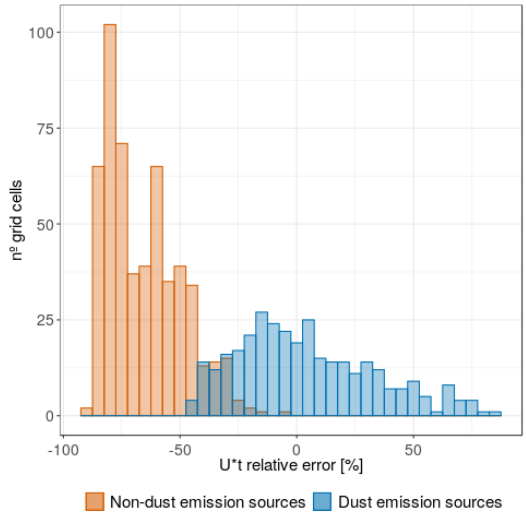

Figure 5. Histogram of the relative error between model and retrieved with the FoO method eorison threshold. Grid cells where there is emission (no-emission) are prensented in blue (red).

The retrieved values for the wind erosion threshold with this method are then compared to those used by the model (bottom Fig.(4)). In areas with no emission, the wind erosion threshold tends to be underestimated by more than around 50% in comparison with the model value (Fig.(5)). On the other hand, dust emission sources show a relative error closer to 0. Over source areas where it has been shown that the FoO of DOD was slightly underestimating the FoO of emissions, the retrieved threshold is then overestimated.

C. Fitting Method

As mentioned in the methodology section, before applying the fits to the DOD data, a filtering to that set of values is previously made with the aim of keeping DOD values that give as much as possible information about the dust being emitted at one location rather than dust that has been transported to there.

If the data set is filtered stepwise with increasing DOD and wind friction velocity and the coefficient of determination (R^2) between DOD and the emission flux is calculated with the remaining data (Fig.(6)), we see that R^2 maximizes with increasing wind friction threshold up to a value around 0.9 m/s. If the wind friction threshold continues increasing, the value of R^2 drops as the number of remaining data after filtering is too low. On the other hand, R^2 does not clearly increase with increasing DOD threshold values.

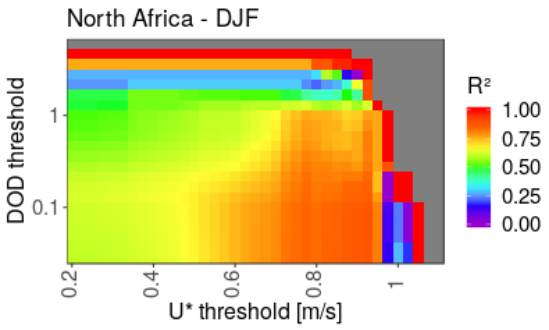

Figure 6. Coefficient of determination between DOD and emission flux for increasing wind friction velocity and DOD thresholds for DJF data.

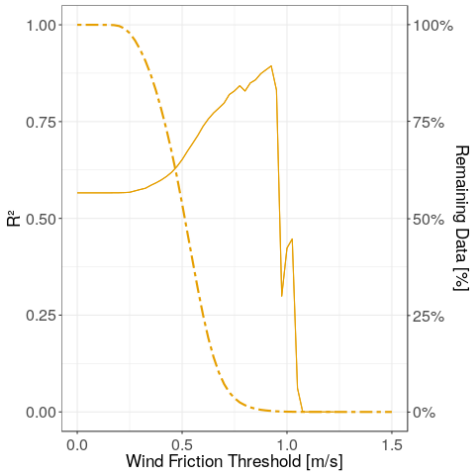

Figure 7. Coefficient of determination between DOD and emission flux for increasing wind friction velocity threshold (solid line) and percentage of initial data that is left after filtering with increasing friction velocity threshold (dashed line).

We decided to select a value of 0.5 m/s as wind friction threshold value for filtering. This selection is based on having having an equilibrium between the R^2 value and the total amount of data remaining after filtering. Although the ideal case would be to use the value in which R^2 maximizes, it is here considered that with the amount of data that is used in this study this filtering would be very restrictive. Meaning that, few points would remain

after applying it at every grid cell so the fitted functions would have a poor statistical significance. So the final selected threshold for filtering is the intersection between the evolution of R^2 with icreasing wind friction threshold and the curve indicating the percentage of remaining data after filtering (Fig.(7)).

Once the filtering is done, the fitting is performed at every grid cell with at least 10 values to assure a minimum significance of the fit. The distribution of the retrieved wind erosion threshold through this method is shown in Fig.(8). The main peculiarity of this resulting distribution is that compared to that obtained with the FoO method, the resulting wind the resulting wind erossion thresholds present a very narrow and low range of values (between 0.2 and 0.5 m/s).

The relative errors of the resulting wind erosion thresholds compared to those used by the model are computed (bottom Fig.(8)). It is shown, that the threshold is overestimated over dust emission sources and underestimated over the other regions where dust is advected as already happened with the FoO method. However, the relative error increases when using this method, both in overestimated and underestimated regions.

To have a closer insight to the possible error sources, data of some particular grid cells and its corresponding fitted function are plotted (Fig.(9)). The selected grid cells correspond to two locations in which dust emissions are given and a third one in which there is no emission. One might detect that the fact of filtering by a given wind friction value is making that the retrieved wind erosion threshold values over emission sources present values in a narrow range around the wind filter threshold (0.5 m/s in this case). Furthermore, over regions with transported dust and no emission, the resulting wind erosion threshold as seen also in Fig.(8) its lower (closer to 0.2 m/s).

The filtering is then not enough efficient to mask regions where there is not dust emission. Because of that, we fit functions to DOD data in places where the initial hypothesis of a proportionality between emission and DOD changes is not at all accomplished. Furthermore, although the DOD tendency with wind is well captured with the fitted function over emission sources, the wind erosion threshold value presents a high dependence on the wind friction threshold selected for filtering.

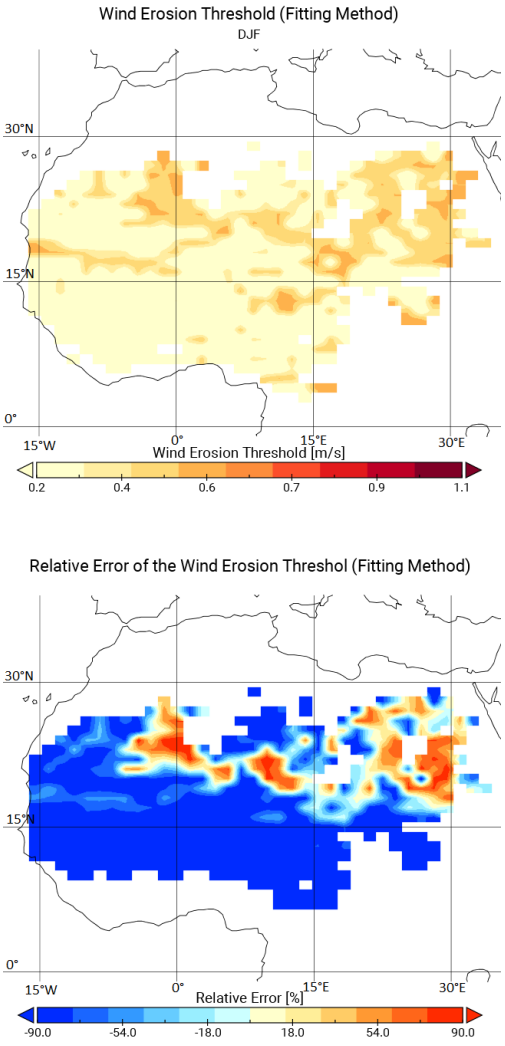

Figure 8. The upper figure presents the wind erosion threshold distribution retrieved through the fitting method using DJF data. In the bottom figure, the relative error between the model-used wind friction threshold velocity and the corresponding retrieved wind erosion threshold for DJF (reddish colors indicate overestimation and blue indicate underestimation).

IV. CONCLUSIONS

With this study, we have been able to assess two different methodologies to infer the wind erosion threshold. The objective was to find a reliable method that could be applied to satellite observations. As there is no way of evaluating the results with satellite data, we have done this assessment with dust model output data.

Based on the results derived from the analysis presented in this work we can conclude that:

- For North Africa, 12 and 15 UTC DOD data presents a higher coefficient of determination with emission fluxes than any other time of the day. And DJF season shows a higher coefficient than any other season.
- When evaluating the FoO method we see that FoO of DOD surpassing 0.2 for DJF is a better approximation of the FoO of emissions than that for JJA or any other season. However, transported dust has the effect of overestimating the FoO of DOD. This fact is then reflected in the wind erosion threshold distribution retrieved, where the threshold is significantly underestimated over regions where transported dust dominates.
- From assessing the second method (fitting method)

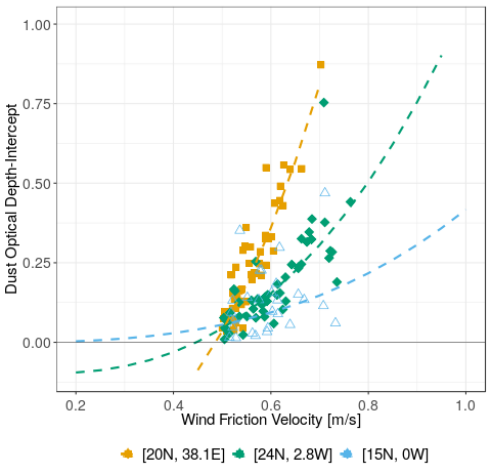

Figure 9. Remaining points of DOD minus background dust after filtering by a 0.5 wind firction value for three different cells. Dashed lines represent the fitted equations. The wind friction threshold found through the fitting method corresponds to the point of intersection of the fitted curve and the coordinate axis. The filled color points represent DOD values in which there was emission at the same time and location and non-filled points represent DOD values in which there was not emission.

> we see that the relative errors are even higher than those from the FoO method. That could be given beacause this method has poor skills when trying to mask transported dust from DOD data.

As future work, the analysis could be done from one region to another depending on the dust source areas, to be able to see if results drastically change. The FoO method has worked better for North Africa, but it relies on a threshold of DOD which might be too high for regions with less emissions. Using a smaller threshold, however, might make it more difficult to unambiguously identify dust source regions. On the other hand, the fitting method did not work well because of the transported dust. In regions with less emission, the transported dust is less dominant and therefore it could be hypothesized that this second method would work better.

It is also important to note that this study has been performed with just a one-year simulation. To have a better estimation of the wind erosion threshold, it would be desired to have longer modeled time-series. In that way, when using the fitting method, more values after filtering would remain at every grid cell and a better fit in terms of statistical significance could be carried out.

Results from both methods clearly show that transported dust is biasing the resulting wind erosion threshold distributions and further research is needed to finer disentangle lateral dust transport from dust being emitted at one place.

ACKNOWLEDGMENTS

I would like to thank Dr. Carlos Pérez and Dr. Martina Klose for introducing me to the captivating world of dust, and for their patience and guidance in writing this project. It has been a pleasure to work hand to hand with them and to be part during this time of a great big team as the Earth Sciences department at the BSC is. I also want to thank Dr. Yolanda Sola and Dr. Mireia Udina from the Barcelona University for their comments.

REFERENCES

Cook, A. G., P. Weinstein, and J. A. Centeno, Health effects of natural dust, *Biological Trace Element Research*, *103*(1), 1–15, 2005.

Cowie, S., P. Knippertz, and J. Marsham, A climatology of dust emission events from northern africa using long-term surface observations, *Atmospheric Chemistry and Physics*, *14*, 2014.

Fécan, F., B. Marticorena, and G. Bergametti, Parameterization of the increase of the aeolian erosion threshold wind friction velocity due to soil moisture for arid and semi-arid areas, *Annales Geophysicae*, *17*, 149–157, doi:10.1007/s00585-999-0149-7, 1999.

Ginoux, P., J. Prospero, T. Gill, N. Christina Hsu, and M. Zhao, Global-scale attribution of anthropogenic and natural dust sources and their emission rates based on modis deep blue aerosol products, *Reviews of Geophysics*, *50*, 3005–, 2012.

Iversen, J., and B. White, Saltation threshold on earth, mars and venus, *Sedimentology*, *29*, 111 – 119, 2006.

Knippertz, P., Dust emissions in the west african heat troughthe role of the diurnal cycle and of extratropical disturbances, *Meteorologische Zeitschrift*, *17*, 553–563, 2008.

Koven, C., and I. Fung, Identifying global dust source areas using high-resolution land surface form, *J. Geophys. Res.*, *113*, D22,204, doi:10.1029/2008JD010195, 2008.

Marticorena, B., and G. Bergametti, Modeling the atmospheric dust cycle. part 1: Design of a soil-derived dust emission scheme, *Journal of Geophysical Research*, *100*, 16,415–16,430, 1995.

Marticorena, B., G. Bergametti, A. Bernard, Y. Callot, C. N'Doum, and M. Legrand, Modeling the atmospheric dust cycle: 2. simulation of saharan dust sources, *Journal of Geophysical Research*, *102*, 4387–4404, doi:10.1029/96JD02964, 1997.

Min, Q.-L., R. Li, B. Lin, E. Joseph, S. Wang, Y. Hu, V. Morris, and F. Chang, Evidence of mineral dust altering cloud microphysics and precipitation, *Atmospheric Chemistry and Physics*, *9*(9), 3223–3231, 2009.

Nicholson, S., The itcz and the seasonal cycle over equatorial africa, *Bulletin of the American Meteorological Society*, *99*, 337–348, doi:10.1175/BAMS-D-16-0287.1, 2018.

N'tchayi Mbourou, G., J. J. Bertrand, and S. Nicholson, The

diurnal and seasonal cycles of wind-borne dust over africa north of the equator, *Journal of Applied Meteorology - J APPL METEOROL*, *36*, 868–882, 1997.

Pauley, P. M., N. L. Baker, and E. H. Barker, An observational study of the "Interstate 5" dust storm case, *Bulletin of the American Meteorological Society*, *77*(4), 693–720, 1996.

Pérez, C., et al., Atmospheric dust modeling from meso to global scales with the online nmmb/bsc-dust model part 1: Model description, annual simulations and evaluation, *Atmospheric Chemistry and Physics*, *11*, 13,001–13,027, 2011.

Prospero, J., P. Ginoux, O. Torres, S. Nicholson, and T. Gill, Environmental characterization of global sources of atmospheric soil dust identified with the nimbus 7 total ozone mapping sectrometer (toms) absorbing aerosol product, *Reviews of Geophysics*, *40*, 2002.

Prospero, J., F.-X. Collard, J. Molinie, and A. Jeannot, Characterizing the annual cycle of African dust transport to the Caribbean Basin and South America and its impact on the environment and air quality, *Global Biogeochemical Cycles*, *28*, 2014.

Pu, B., et al., Retrieving the global distribution of threshold of wind erosion from satellite data and implementing it into the gfdl am4.0/lm4.0 model, *Atmospheric Chemistry and Physics Discussions*, pp. 1–74, 2019.

Shao, Y., and H. Lu, A simple expression for wind erosion threshold friction velocity, *Journal of Geophysical Research*, *105*, 22,437–22,443, 2000.

Shao, Y., M. Klose, and K.-H. Wyrwoll, Recent global dust trend and connections to climate forcing, *Journal of Geophysical Research: Atmospheres*, *118*(19), 11,107–11,118, 2013.

Solomon, S., D. Qin, D. Manning, Z. Chen, M. Marquis, K. B. Averyt, M. Tignor, and H. L. Miller, IPCC, 2007: Climate Change 2007: The Physical Science Basis. Contribution of Working Group I to the Fourth Assessment Report of the Intergovernmental Panel on Climate Change, *Cambridge University Press, Cambridge, United Kingdom and New York, NY, USA*, 2007.

White, B., Soil transport by winds on mars, *Journal of Geophysical Research*, *84*, 1979.

Wittmann, M., C. D. Groot Zwaaftink, L. Steffensen Schmidt, S. Gumundsson, F. Pálsson, O. Arnalds, H. Björnsson, T. Thorsteinsson, and A. Stohl, Impact of dust deposition on the albedo of vatnajökull ice cap, iceland, *The Cryosphere*, *11*(2), 741–754, 2017.

Woodward, S., Modeling the atmospheric life cycle and radiative impact of mineral dust in the Hadley Centre climate model, *Journal of Geophysicall Research*, *106*(D16), 18,155–18,166, 2001.